An X-Ray Absorption Spectroscopy Study of the Zinc Environment in Langmuir-Blodgett Phospholipid Multilayers

S. Nuzzo,* C. Meneghini,[†‡] S. Mobilioo,[‡§] H. Haas,[¶] P. Riccio,[‖] A. Fasano,[**] P. Cavatorta,[††‡‡] and S. Morante[‡‡§§]

*Dipartimento di Fisica, University of Napoli, Italy; [†]INFM General Purpose Italian Beam Line for Diffraction and Absorption c/o European Synchrotron Radiation Facility Grenoble, France; [‡]Dipartimento di Fisica Universita' Roma Tre, Italy; [§]Laboratori Nazionali di Frascati dell' INFN, Frascati, Italy; [¶]MBT Munich Biotechnology GmbH, Martinsried, Germany; [‖]Dipartimento di Biologia, D.B.A.F., University of Basilicata, Potenza, Italy; **Dipartimento di Biochimica e Biologia Molecolare, University of Bari, Italy; [††]Dipartimento di Fisica, University of Parma, Italy; [‡‡]Istituto Nazionale per la Fisica della Materia, Italy; and [§§]Dipartimento di Fisica, University of Roma Tor Vergata Roma, Italy

ABSTRACT For the first time x-ray absorption spectroscopy was used to investigate the Zn environment in Langmuir-Blodgett multilayers. The multilayers were taken as a model of the multilamellar structure of the myelin sheath, the membrane surrounding the nerve axon, which plays a crucial role for signal transduction along the axon. The layers were assembled from the phospholipid dilauroylphosphatidic acid, both in the presence and in the absence of myelin basic protein. The analysis of the extended x-ray absorption fine structure and of the near edge regions of the x-ray absorption spectra at the Zn K-edge provided an accurate description of the local structure showing that the Zn ions are bound to the heads of the phospholipid molecules. The myelin basic protein induces a distortion on the Zn local environment due to a steric constraint but does not substitute the phosphate headgroups. These findings represent an important step in understanding the interplay among myelin basic protein, Zn, and the lipids of the myelin sheath.

INTRODUCTION

The myelin sheath of the central nervous system is a multilamellar membrane formed by several lipid bilayers tightly wrapped around the nerve axon. Its integrity is crucial for an efficient transduction of signals along the axon. The myelin basic protein (MBP) plays an important role in ensuring the stability of the central nervous system myelin sheath (Boggs and Moscarello, 1982; Riccio et al., 1986, 2000). Its capability in preserving the compactness and the stability of the myelin membrane seems to be enhanced by the presence of Zn ions (Inouye and Kirschner, 1984; Berlet et al., 1987; Earl et al., 1988). In fact, Zn stabilizes the "in vitro" self-association of MBP dissolved in phosphate buffer (Cavatorta et al., 1994); however, there are only few evidences that Zn binds to MBP (Riccio et al., 1995), probably in a site involving the histidines of the protein (Zhang et al., 1997). On the other hand, it is well known that both Zn and MBP bind to the lipid membrane through electrostatic interactions and strongly modify its structure (Boggs and Moscarello, 1982; Smith, 1992; Haas et al. 1998). However, up to now, a full understanding of the structural and functional interplay between Zn, MBP, and the lipid membrane is still missing. To elucidate this interplay, accurate information on the interaction between Zn ions and the components of the myelin sheath are necessary.

Monolayers at the air/water interface may be used to investigate the interaction between MBP and phospholipids. In fact, using floating monolayers as precursors, protein/lipid multilayers can be assembled on solid substrates (Langmuir-Blodgett multilayers, LBMLs), and these LBML quite accurately model the multilamellar structure of the myelin sheath. The molecular organization of the LBML has been previously investigated in detail by a number of experimental techniques like x-ray and neutron scattering, Fourier transform infrared spectroscopy, and circular dichroism (Haas et al., 1998). In particular surface sensitive techniques allow obtaining structural information up to the submolecular level (Moehwald, 1990). Among these techniques, grazing incidence x-ray scattering with synchrotron radiation provides the vertical profile of the membranes as well as the in-plane molecular packing (Als-Nielsen and Möhwald, 1991; Jaquemain et al., 1992; Helm et al. 1991; Haas et al., 1995). However, so far, even these methods failed to provide insight into structural details of the lipid headgroup region, which is very relevant in biology.

In this article, we demonstrate that x-ray absorption spectroscopy (XAS) provides this information. XAS is the ideal tool to obtain information about the local environment around a specific atomic species (Lee et al., 1981). We report here on XAS measurements carried out to determine the local structure of Zn ions embedded in LBMLs in the absence and in the presence of MBP. Zn ions were bound to the phosphate headgroups of the lipid molecules with a local geometry strongly modified by the presence of water (swelling) and myelin basic protein.

MATERIALS AND METHODS

Sample preparation

L-α-Dilauroylhosphatidic acid (Sigma, Munich, Germany) was spread from a chloroform:methanol solution, 3:1 (Merck, Darmstadt, Germany),

Submitted September 14, 2001, and accepted for publication July 3, 2002.

Address reprint requests to Prof. Settimio Mobilio, Dipartimento di Fisica "E. Amaldi," Universita' Roma Tre, Via della Vasca Navale 84, 00146 Roma, Italy. Tel.: 0039-6-94032288; Fax: 0039-6-94032304; E-mail: mobilio@lnf.infn.it.

0006-3495/02/12/3507/06 $2.00

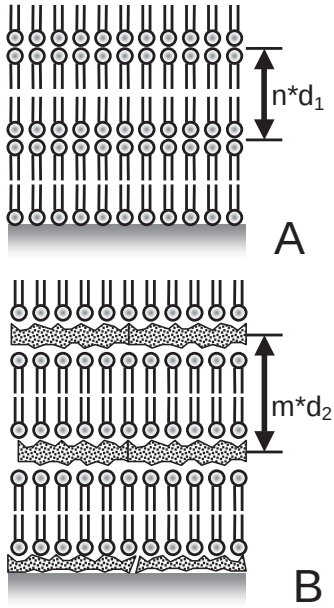

FIGURE 1 Molecular organization of the lipid (*a*) and protein/lipid (*b*) multilayers. The samples, assembled by layer-by-layer deposition from the liquid interface, can be described as repeating planar bilayers with a single top layer whose hydrocarbon chains are oriented toward the air. In case of the protein/lipid samples, the protein (represented by the vertical blocks) is inserted between adjacent headgroups.

on a subphase of a 10^{-3} M solution of $ZnCl_2$ (Merck) and on a subphase of a 10^{-3} M solution of $ZnCl_2$ with addition of 5×10^{-8} M of MPB. The subphase solutions were made from Milli-Q (Millipore, Bedford, MA) filtered water (pH 5.5).

MBP was purified in the water-soluble, lipid-free form according to established procedures (Deibler et al., 1972, 1984). Protein content was determined using the Bio-Rad Bradford reagent (Bio-Rad Laboratories, Hercules, CA) and the micro assay procedure.

The floating phospholipid monolayers were transferred by Langmuir-Blodgett deposition on hydrophilic Kapton foil. Before deposition, the Kapton was cleaned by sonication with detergents and by extensive rinsing. During deposition, the surface pressure was 40 mN/m^2, and the deposition rate 10 mm/min. The deposition of the protein/lipid layers was performed after waiting 4 h, and the protein adsorption was monitored measuring the surface pressure. Twenty-three layers were deposited for the phospholipid sample and 21 layers for the protein/lipid sample. In each case, well-ordered multilayers were achieved with well-defined Kiessig-fringes and Bragg peaks in x-ray reflectivity spectra, measured on similarly prepared samples on glass substrates. From the Bragg peaks in the pure lipids sample a bilayer spacing of 4.4 nm was measured, whereas in the L-α-dilauroyl-hosphatidic acid/MBP sample the spacing was 6.2 nm.

The molecular organization in the multilayers is sketched in Fig. 1. The pure lipid samples consist of repeating lipid bilayers and a single top layer with hydrocarbon chains oriented toward air. In the lipid/protein samples, the protein is inserted between adjacent headgroups, leading to an increase of bilayer spacing.

XAS measurements

X-ray absorption spectroscopy measurements were performed at the Italian beamline GILDA (general purpose Italian beam line for diffraction and absorption) (Pascarelli et al., 1996) of the European synchrotron radiation facility in Grenoble (France). Spectra were recorded at the Zn K edge in the energy range 9500 to 10,100 eV. The beam was monochromatized by a Si[311] double crystal monochromator operating in the dynamical sagittal focusing mode (Pascarelli et al., 1996), which provides a small ($\approx$2 mm^2), intense ($\sim 10^{11}$ photons/s), and stable spot on the sample. The energy resolution was $\sim$0.4 eV. To reject the harmonics two Pd-coated mirrors were placed one upstream and the other downstream the monochromator (cutoff energy of $\sim$24 KeV). Spectra were recorded at room temperature, in fluorescence geometry, using a seven-element Ge solid-state detector to isolate the Zn K_α fluorescence from other unwanted contributions. For data normalization, the incident photon flux was monitored using an N_2-filled ionization chamber.

Two samples were studied, the multilayers in absence of MBP (measurements s_a and s_b) and in presence of MBP (measurement s_c and s_d). Both samples were measured in air (s_a and s_c) and in a vacuum of $\sim 10^{-5}$ bar (s_b and s_d).

As reference sample, a 10^{-3} M water solution of $ZnSO_4$ was used.

Data analysis

For the data analysis, it is necessary to treat separately the XANES (x-ray absorption near edge structure) region and the EXAFS (extended x-ray absorption fine structure) region of the spectrum. The XANES region extends from the absorption edge up to few tens of electron volts above it, on the other hand, the EXAFS starts from few tens of electron volts and extends up to several hundreds of electron volts above.

Let us first discuss the extended region. The EXAFS spectrum, $\chi(k)$, is defined by the formula:

$$\chi(k) = \frac{\mu(k) - \mu_0(k)}{\mu_0(k)} \tag{1}$$

in which $\mu(k)$ is the measured absorption coefficient of the material under study, and $\mu_0(k)$ is the atomic absorption coefficient. k is the modulus of the photoelectron wave vector emitted in the absorption process; its value is related to the energy of the incident photon, E, by the relation:

$$k = \frac{\sqrt{2m(E - E_0)}}{\hbar} \tag{2}$$

in which E_0 is the absorption threshold.

In the EXAFS region, k is greater than $\sim$2 Å^{-1}, and the spectrum $\chi(k)$ of Eq. 1 is described by the formula:

$$\chi(k) = S_0^2 \sum_i \frac{N_i}{kR_i^2} A_i(k) \exp(-2k^2\sigma_i^2) \exp\left(-\frac{2R_i}{\lambda}\right) \times \sin[2kR_i + \phi_i(k)] \tag{3}$$

valid within the single scattering approximation (Lee et al., 1981).

In Eq. 3, the sum is over all the different coordination shells surrounding the absorption atom, N_i is the number of atoms belonging to the ith coordination shell, located at a distance R_i from the absorber. The exponential factor $\exp(-2k^2\sigma_i^2)$, the so-called Debye-Waller factor, takes into account the static and/or dynamic fluctuations of the position of the scatterers in the ith shell. The term $\exp(-2R_i/\lambda)$ takes into account the mean free path of the extracted photoelectron, which is limited by the inelastic collisions with the other electrons and by the core-hole lifetime. S_0^2 is a factor that accounts for an overall reduction of the signal due to many-body effects. $A_i(k)$ is the modulus of the back-scattering amplitude and $[2kR_i + \phi_i(k)]$ is the total scattering phase associated to the ith coordination shell. The structural information of the spectra consists of the distances, coordination numbers, and Debye Waller factors of the different coordination shells surrounding the absorbing atom. Such information can be deduced from the spectra only after the other factors

$A_i(k)$, $\phi_i(k)$, S_0^2, $\lambda(k)$ have been determined either from theoretical calculation or experimentally.

The EXAFS data analysis was performed using the GNXAS package (Filipponi et al., 1995; Filipponi and Di Cicco, 1995), which also includes effects coming from multiple scattering effects not considered in Eq. 3 (Benfatto et al., 1986). In this package, a theoretical absorption coefficient, $\mu_{TH}(k)$, evaluated using Eq. 1 is fitted to the measured absorption coefficient $\mu_{EXP}(k)$. In evaluating $\mu_{TH}(k)$, the theoretical structural signal, $\chi_{TH}(k)$ is calculated assuming a structural model composed of one or more coordination shells around the absorber; the atomic background, $\mu_0(k)$, is modeled using polynomial splines. The best fit values of the structural parameters present in $\chi_{TH}(k)$, i.e., R_i, N_i, and σ_i, are obtained by minimizing the quantity:

$$R = \frac{M}{M-P}\frac{\sum_k (\mu_{EXP}(k) - \mu_{TH}(k))^2}{\sum_k (\mu_{EXP}(k))^2} \qquad (4)$$

the sum is over the M measured values of k, and P is the number of free parameters appearing in the parametrization of $\mu_{TH}(k)$.

Our data were fitted very well with a model composed of only two coordination shells. The fitting procedure gave for each shell the three parameters, N_i number of atoms in the i-shell, R_i their average distance from the Zn, and the corresponding Debye-Waller factor σ_i^2. Multiple scattering effects were found to be negligible.

In the XANES region of the spectrum, electronic processes like transitions to bound states as well as multiple scattering effects are not negligible. As a consequence, the structure of the XANES region is very sensitive to the electronic structure of the central atom and to the symmetry of the local environment around the absorber (Benfatto et al., 1986). Due to the presence of all these processes, the quantitative interpretation of this part of the spectrum is very difficult. Despite these problems, the comparison of XANES spectra of structurally similar samples can be used to obtain information on similarities and differences in their local geometry (Bianconi et al., 1986).

RESULTS

Fig. 2 reports the absorption coefficient, μ_{EXP} of the four multilayer samples and of the reference sample. Fig. 3 reports the Fourier transform of the EXAFS spectra. From both figures, it is clear that in the EXAFS region all the spectra of the multilayer samples are rather similar one to the other but significantly different from the reference sample. This demonstrates that the local coordination around Zn is very similar in all the samples and that it is definitely different from that of Zn ions in water solution.

On the other hand, significant differences were present among the XANES spectra of the four samples (Fig. 4). In fact, apart from the main peak known as "white line," which is present in all the spectra, an additional shoulder at lower energy is evident in the sample with MBP measured under vacuum. With a lower intensity, the same additional peak is present also in the spectrum of the same sample measured in air and in that of the sample without protein measured in vacuum. These variations are a clear indication that the local order around the Zn atoms is not identical in all the samples. In fact, in a systematic study on the XANES of many different Zn compounds, Jacquament et al. (1998) showed that the relative intensity of the secondary shoulder with respect to the height of the "white-line" depends on the geometrical arrangement of the ligands around Zn, on their chemical nature, and on their number. From this study, we conclude that the Zn local geometry evolves from a tetrahedral to a planar geometry either by adding MBP or by lowering the pressure.

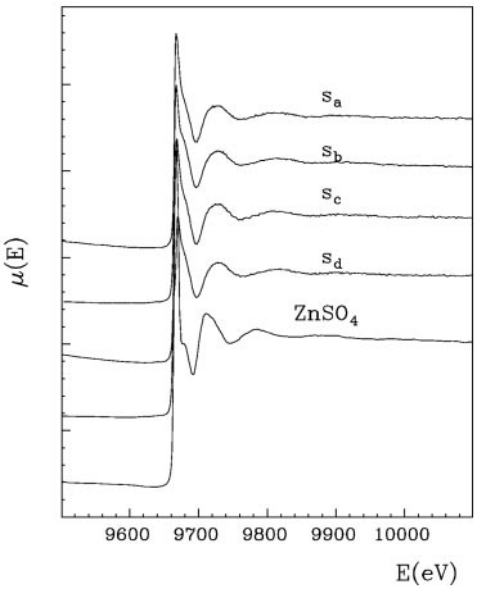

FIGURE 2 Experimentally measured absorption coefficients μ plotted as function of the photoelectron energy E in eV of the four sample and of the reference sample. Samples are labeled as: s_a, LBML in absence of MBP in air; s_b, LBML in absence of MBP in vacuum; s_c, LBML in presence of MBP in air; and s_d, LBML in presence of MBP in vacuum. Zn concentration was 10^{-3} M, MBP concentration 10^{-8} M, pH 5.5.

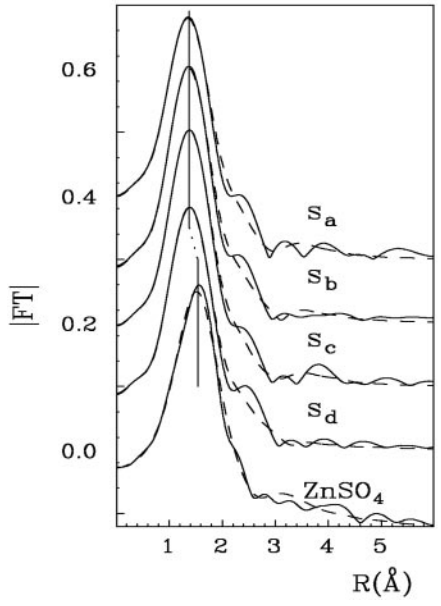

FIGURE 3 Fourier transform of the EXAFS spectra of the four samples s_a to s_c and of the reference sample.

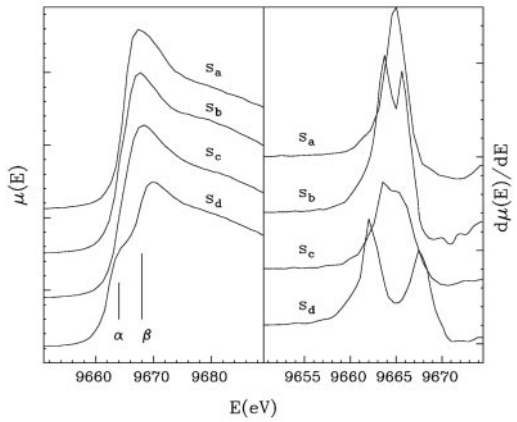

FIGURE 4 Blow up of the XANES region of the spectra of Fig. 2 (*a*) and of their first derivatives (*b*).

To clarify the differences between the local structure of the samples, we carried out a quantitative analysis of the EXAFS spectra. For each sample, a theoretical spectrum composed of two oxygen shells surrounding the Zn atoms was fitted to the experimental spectrum (Fig. 5). In Fig. 6, the contribution of the two shells for sample s_c are separately plotted to give an idea of their different weight on the total spectrum; the contribution of the second shell, although fairly small, is not negligible and must be included in the analysis to obtain a good fit in terms of the χ^2 value. For the other samples, a similar situation was found. To show the quality of the fitting procedure (Fig. 6), the residual signal is reported also.

In Table 1, the values obtained for the structural parameters are reported; errors are given in parenthesis. For comparison, the structural parameters obtained by fitting the data of the $ZnSO_4$ reference sample also are reported. The

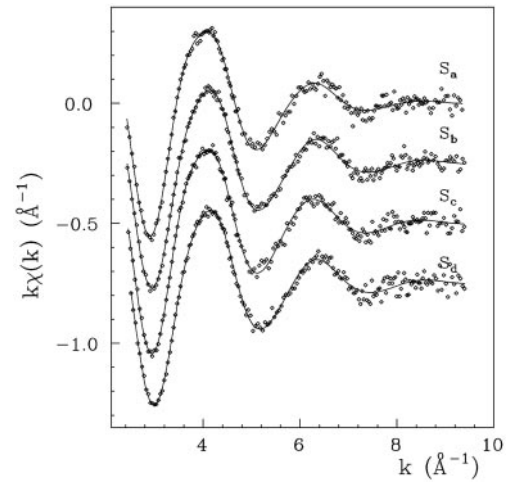

FIGURE 5 Experimental EXAFS signal, $\chi_{EXP}(k)$ (*diamonds*) and, superimposed to it, the total theoretical signal, $\chi_{TH}(k)$ (*solid line*) for the four samples. Experimental and theoretical data have been multiplied by *k*.

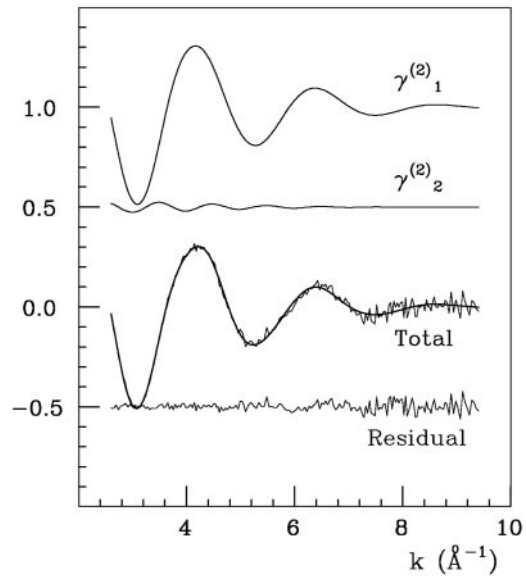

FIGURE 6 Two contributions to $\chi_{EXP}(k)$ separately plotted as functions of *k* as determined by fitting the data of sample s_c. The residual signal is also shown at the bottom of the figure.

two oxygen coordination shells are located at $R_1 \approx 1.95$ Å and $R_2 \approx 3.4$ Å from the Zn absorber, respectively. The first one contains four oxygen atoms and the second only one to two. The more distant coordination shell is characterized by larger Debye Waller value, which is indicative of a bigger structural disorder.

It is very clear that the values of the structural parameters of the four multilayer samples are very different from those of Zn solution in water: four oxygen atoms are found instead of six at a distance, which is 0.1 Å shorter. Furthermore, the higher σ^2 values indicate that a larger structural disorder in the Zn environment is present. It is worth noticing that the large disorder of the next neighbor shell may mask a distribution of distances more complex that a simple Gaussian; however, the weakness of this contribution prevents the possibility to shed light on this aspect.

TABLE 1 Values of the structural parameters resulting from the fitting of the spectra of the four samples and of the reference sample, $ZnSO_4$

Sample	N_1	R_1 (Å)	σ_1^2 (Å^2 × 100)	N_2	R_2 (Å)	σ_2^2 (Å^2 × 100)
s_a	3.9(3)	1.96(2)	0.55(5)	1.3(2)	3.35(5)	1.1(2)
s_b	3.7(3)	1.95(2)	0.33(5)	1.4(3)	3.39(5)	1.0(2)
s_c	3.7(3)	1.96(2)	0.33(5)	1.5(3)	3.37(5)	1.3(2)
s_d	3.7(3)	1.95(2)	0.35(5)	1.3(2)	3.40(5)	1.1(2)
$ZnSO_4$	6.0(4)	2.07(2)	0.11(3)	2.9(2)	3.33(5)	1.5(2)

N_i is the coordination number of the *i*th coordination shell, R_i its distance from Zn, and σ_i its Debye Waller factor. Errors are given in parenthesis.

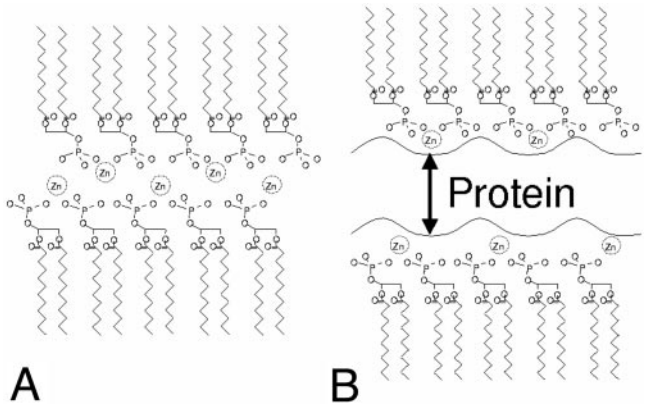

FIGURE 7 Schematic molecular model for the configuration of the Zn ions in the headgroup slab of the bilayers. For clarity water molecules are not shown. (*a*) Lipid bilayer. (*b*) Lipid/protein bilayer.

DISCUSSION

As shown above, from the EXAFS spectra we conclude that, concerning the number and the chemical nature of the ligands, the short range atomic environment around the Zn ions is almost identical in all the samples. From the XANES, we conclude that the presence of MBP in the LBMLs induces a geometrical distortion of the Zn local environment from a tetrahedral-like to a planar-like geometry and that a similar distortion is induced or enhanced also by lowering the pressure.

As already discussed in the Introduction, LBML-MBP assemblies have been extensively studied by means of many different experimental techniques (Haas et al., 1998). The data were consistent with a model in which the protein is well packed in a sandwich-like structure of the type "headgroups-protein-headgroups," with a small amount of water present inside. In presence of the protein the head-head spacing was ~10 Å (Haas et al., 1998). This is almost exactly the space occupied by the protein lying flat between the headgroups of the lipid matrix. In absence of the protein, the head-head spacing was somewhat reduced, coming down to approximately a few Ångstroms. On these grounds, Zn ions should be located in the hydrophilic medium between the phospholipid heads of two adjacent layers, as schematically depicted in Fig. 7 *a*. The headgroups of lipids in the two layers face each other so that the Zn ions may coordinate up to four oxygen atoms of the phosphate groups. In addition, as known from neutron reflectivity, water molecules also are present between the layers (Haas et al., 1999). Therefore, Zn may be coordinated with the oxygen of the water molecules and/or the oxygen of the phosphate headgroups.

Within this picture, we suggest that Zn ions coordinate the oxygen of the phosphate groups in the first coordination sphere. The evolution of the local geometry from a tetrahedral to a planar one upon lowering the pressure is due to the removal of the water molecules that makes the LBML structure more tightly packed in the head region.

In presence of MBP, a similar distortion occurs, leading to a picture of the molecular assembly as that depicted in Fig. 7 *b*. Also in this case, the Zn atoms are bound to the phosphate heads; the presence of the protein induces an even larger steric constraint, modifying the local geometry of the Zn environment. This hypothesis is supported by the observation that with lowering the pressure, a larger distortion occurs due to a larger steric constraint induced by the removal of the water molecules.

An additional question arises on a possible direct bond between MBP and Zn. It is known that in the presence of inorganic phosphate Zn causes the aggregation of MBP (Cavatorta et al., 1994). This influence may be due either to a cooperative effect of the interaction between the various components or to the binding of Zn to a specific site in the protein. MBP contains 10 histidines that in principle may bind Zn ions; in particular, in the MBP sequence the characteristic Zn-finger binding motif, His-X-X-His, is present (Cavatorta et al., 1994). The hypothesis of the existence of a specific binding site for Zn in MBP was supported by Riccio et al. (1995). In addition Zhang et al. (1997) demonstrated that the histidine residues are involved in the Zn binding by showing that the chemical modification of these residues completely eliminates such binding.

It is well known (Bunker et al., 1982; Blackburn et al., 1983; Strange et al., 1987) that coordinated histidines give rise to large MS contributions (from the nearby presence of histidine imidazoles), producing a peak in the FT at ~3.5 Å (Meneghini and Morante, 1998). One might expect that the existence of this kind of binding should be easily detectable by XAS measurements. As shown in Fig. 3, none of the FTs has evidence of an enhancement in this region.

However, in our experimental conditions, the maximum expected concentration of Zn atoms bound to MBP would be too low to be detectable. In fact, from the experimental conditions during Langmuir-Blodgett transfer, the area for each lipid head is estimated of the order of 40 $Å^2$. MBP, lying flat between two adjacent lipid layers, occupies an area of $\sim 150 \times 15$ $Å^2$ (Haas et al., 1998). There are ~100 lipid heads in the near vicinity of each MBP molecule. Because electric neutrality requests that there is approximately one Zn ion for each lipid head, we conclude that the ratio, *r*, of Zn atoms bound to the protein over Zn atoms bound to the lipid heads is:

r = (MBP-bound-Zn atoms)/(head-bound-Zn atoms) = 0.01

With such a low value a possible signal coming from Zn bound to the MBP protein is not detectable, being overwhelmed by the signal coming from Zn bound to the lipid heads.

Therefore, the changes we observe in the local coordination around Zn are not due to a direct binding between Zn and MBP but to an indirect steric effect.

The most obvious way to make a possible Zn-MBP binding visible is to increase the ratio *r* by reducing the Zn concentration in LBMLs. However, this seems nowadays prohibitive in terms of beam time needed for the XAS measurements.

We thank V. Minicozzi for helping us in preparing the figures. P.R. and A.F. acknowledge the funding from the Italian Foundation for Multiple Sclerosis (FISM). The Italian Institutions CNR, INFM, and INFN fund the General Purpose Italian Beam Line for Diffraction and Absorption Beamline. The technical help of F. Campolungo, V. Sciarra, and V. Tullio (LNF-INFN) for the beam-line set up is greatly appreciated.

REFERENCES

Als-Nielsen, J., and H. Möhwald. 1991. Synchrotron x-ray scattering studies of Langmuir films. *In* Handbook of Synchrotron Radiation, Vol. 4. S. Ebashi, M. Koch, and E. Rubinstein, editors. Elsevier, North-Holland. 1–54.

Benfatto, M., C. R. Natoli, A. Bianconi, J. Garcia, A. Marcelli, M. Fanfoni, and I. Davoli. 1986. Multiple scattering regime and higher-order correlations in x-ray absorption spectra of liquid solutions. *Phys. Rev. B.* 34:5774–5781.

Berlet, H. H., H. Ilzenhofer, and M. Noue. 1987. Metal cations and binding of extrinsic protein of bovine myelin. *Biol. Chem.* 378:1246–1249.

Bianconi, A., A. Congiu-Castellano, M. Dell'Ariccia, A. Giovannelli, S. Morante, E. Burattini, and P. J. Durham. 1986. Local Fe site structure in the tense-to-relaxed transition in Carp deoxyhemoglobin: a XANES (x-ray absorption near edge structure) study. *Proc. Natl. Acad. Sci. U. S. A.* 83:7736–7740.

Blackburn, N. J., S. S. Hasnain, G. P. Diakun, P. F. Knowles, N. Binsted, and C. D. Garner. 1983. An extended x-ray absorption fine structure study of the copper and Zn sites of freeze-dried bovine superoxide dismutase. *Biochem. J.* 213:765–768.

Boggs, J. M., and M. A. Moscarello. 1982. Structural organization of myelin: role of lipid-protein interactions determined in model system. *In* Lipid-Protein Interactions. Vol. 2. P. C. Jost and O. H. Griffith, editors. John Wiley and Sons, New York. 1–51.

Bunker, G., E. A. Stern, R. E. Blankeship, and W. W. Parson. 1982. An x-ray absorption study of the iron site in bacterial photosynthetic reaction center. *Biophys. J.* 37:539–551.

Cavatorta, P., S. Giovanelli, A. Bobba, P. Riccio, A. G. Szabo, and E. Quagliarello. 1994. Myelin basic protein interaction with Zn and phosphate: fluorescence studies on the water-soluble form of the protein. *Biophys. J.* 66:1174–1179.

Deibler, G. E., L. F. Boyd, and M. W. Kies. 1984. Proteolytic activity associated with purified myelin basic protein. *In* Experimental Allergic Encephalomyelitis: A Useful Model for Multiple Sclerosis. E. C. Alvord, Jr., M. W. Kies, and A. J. Suckling, editors. Alan R. Liss, Inc, New York. 249–256.

Deibler, G. E., R. E. Martenson, and M. W. Kies. 1972. Large-scale preparation of myelin basic protein from central nervous tissue of several mammalian species. *Prep. Biochem.* 2:139–165.

Earl, C. E., A. C. Chantry, N. Mohammad, and P. Glynn. 1988. Zn ions stabilize the association of basic protein with brain myelin membranes. *J. Neurochem.* 51:718–724.

Filipponi, A., and A. Di Cicco. 1995. X-ray absorption spectroscopy and n-body distribution functions in condensed matter: II. Data analysis and applications. *Phys. Rev. B.* 52:15135–15149.

Filipponi, A., A. Di Cicco, and C. R. Natoli. 1995. X-ray absorption spectroscopy and n-body distribution functions in condensed matter. *I. Theory. Phys. Rev. B.* 52:15122–15134.

Haas, H., G. Brezesinski, and H. Moehwald. 1995. X-ray diffraction of a protein crystal anchored at the air/water interface. *Biophys. J.* 68: 312–314.

Haas, H., N. Lanteri, and R. Steitz. 1999. BENSC Experimental Report 1999.

Haas, H., M. Torrielli, R. Steitz, P. Cavatorta, R. Sorbi, A. Fasano, P. Riccio, and A. Gliozzi. 1998. Myelin model membranes on solid substrates. *Thin Solid Films.* 327–329:627–631.

Helm, C. A., P. Tippmann-Krayer, H. Moehwald, J. Als-Nielsen, and K. Kjaer. 1991. Phases of phosphatidyl etaholamine monolayers studied by synchrotron X-ray scattering. *Biophys. J.* 60:1457–1476.

Inouye, H., and D. A. Kirschner. 1984. Effects of ZnCl2 on membrane interactions in myelin of normal and shiverer mice. *Biochim. Biophys. Acta.* 776:197–208.

Jacquament, L., D. Aberdam, A. Adrait, J.-L. Hazemann, J.-M. Latour, and I. Michaud-Soret. 1998. X-ray absorption spectroscopy of a new Zn site in the fur protein from *Escherichia coli*. *Biochemistry.* 37:2654–2671.

Jaquemain, D., S. Grayer-Wolf, F. Leveiller, M. Deutsch, K. Kjaer, J. Als-Nielsen, and Leiserowitz, L. 1992. Two-dimensional crystallography of amphiphilic molecules at the air-water-interface. *Angew. Chem. Int. Ed.* 31:130–152.

Lee, P. A., P. H. Citrin, P. Einsenberg, and B. M. Kincaid. 1981. Extended x-ray absorption fine structure: its strengths and limitations as a structural tool. *Rev. Mod. Phys.* 53:769–806.

Meneghini, C., and S. Morante. 1998. The active site structure of tetanus neurotoxin resolved by multiple scattering analysis in x-ray absorption spectroscopy. *Biophys. J.* 75:1953–1963.

Moehwald, H. 1990. Phospholipid and phospholipid-protein monolayers at the air water interface. *Annu. Rev. Phys. Chem.* 41:441–476.

Pascarelli, S., F. Boscherini, F. D'Acapito, J. Hardy, C. Meneghini, and S. Mobilio. 1996. X-ray optics of a dynamical sagittal-focusing monochromator on the GILDA beam line at the ESRF. *J. Synchr. Rad.* 3:147–155.

Riccio, P., N. Borenshtein, A. Fasano, T. Bleve-Zacheo, and D. A. Kirschner. 2000. Multilamellar packing of myelin modeled by lipid-bound MBP. *J. Neurosci. Res.* 59:513–521.

Riccio, P., S. Giovannelli, A. Bobba, E. Romito, A. Fasano, T. Bleve-Zacheo, R. Favilla, E. Quagliariello, and P. Cavatorta. 1995. Specificity of zinc binding to myelin basic protein. *Neurochem. Res.* 20:1107–1113.

Riccio, P. L., L. Masotti, P. Cavatorta, A. De Sanctis, D. Juretic, A. Bobba, I. Pasquali-Ronchetti, and E. Quagliarello. 1986. Myelin basic protein ability to organize lipid bilayers: structural transition in bilayers of lysophosphatidylcholine micelles. *Biochem. Biophys. Res. Commun.* 134:313–319.

Smith, R. 1992. The basic protein of CNS myelin: its structure and ligand binding. *J. Neurochem.* 59:1589–1608.

Strange, R. W., N. J. Blackburn, P. F. Knowles, and S. S. Hasnain. 1987. X-ray absorption spectroscopy of metal-histidine coordination in metalloproteins: exact simulation of the EXAFS of tetrakis(imidazole) copper(II) nitrate and other copper-imidazole complexes by the use of a multiple-scattering treatment. *J. Am. Chem. Soc.* 109:7157–7162.

Zhang, H. H., A. Filipponi, A. Di Cicco, M. J. Scott, R. H. Holm, B. Hedman, and K. O. Hodgson. 1997. Multiple edge XAS studies of cyanide-bridged iron-copper molecular assemblies relevant to cyanide-inhibited heme-copper oxydases using four-body multiple scattering analysis. *J. Am. Chem. Soc.* 119:2470–2478.